Measurement report: Surface exchange fluxes of HONO during the growth process of paddy fields in the Huaihe River Basin, China

Fanhao Meng[1,3,a], Baobin Han[1,2,a], Min Qin[1], Wu Fang[1,8], Ke Tang[4], Dou Shao[1,2], Zhitang Liao[1,2], Jun Duan[1], Yan Feng[5,6], Yong Huang[5,6], Ting Ni[5,6], Pinhua Xie[1,2,7,8]

[1] Key Laboratory of Environmental Optics and Technology, Anhui Institute of Optics and Fine Mechanics, Hefei Institutes of Physical Science, Chinese Academy of Sciences, Hefei, 230031, China

[2] University of Science and Technology of China, Hefei, 230026, China

[3] State Key Laboratory of Pulsed Power Laser Technology, National University of Defense Technology, Hefei 230037, China

[4] School of Electrical and Photoelectronic Engineering, West Anhui University, Luan 237012, China

[5] Anhui Institute of Meteorological Sciences, Anhui Province Key Laboratory of Atmospheric Science and Satellite Remote Sensing, Hefei 230031, China

[6] Shouxian National Climatology Observatory, Huaihe River Basin Typical Farm Eco–meteorological Experiment Field of CMA, Shouxian 232200, China

[7] CAS Center for Excellence in Regional Atmospheric Environment, Institute of Urban Environment, Chinese Academy of Sciences, Xiamen, 361021, China

[8] Institute of Environment, Hefei Comprehensive National Science Center, Hefei 230031, China

[a] These authors contributed equally to this work.

Correspondence to: Min Qin (mqin@aiofm.ac.cn)

Abstract: Significant amounts of nitrous acid (HONO) released from soil affect the chemistry of the troposphere, as a major precursor of hydroxyl radical. However, the scarcity of in-situ data on soil–atmosphere HONO exchange flux has constrained the comprehension of emission mechanisms and reactive nitrogen budget. Herein, we performed measurements of HONO and NO_x fluxes over paddy fields in the Huaihe River Basin. The entire experiment experienced various agricultural management activities, including rotary tillage, flood irrigation, fertilization, paddy cultivation and growth, and top-dressing. HONO and NO exhibited more upward fluxes, whereas NO_2 deposited to the ground, with average hourly fluxes of 0.07 ± 0.22, 0.19 ± 0.53 and -0.42 ± 0.44 nmol m^{-2} s^{-1}, respectively. Continuous peaks in HONO and NO fluxes were observed during the rotary tillage, and they exhibited a significant correlation ($R = 0.77$). Moreover, a significant correlation ($R = 0.60$) between HONO flux and the product of $J(NO_2) \times NO_2$ was also observed during the daytime. The results indicate that both soil biological emissions and light-driven NO_2 conversion are likely active, collectively influencing the diurnal pattern of HONO flux. Source analysis revealed that the unknown HONO source (P_{unknown}) exhibited a diurnal pattern with higher daytime and lower nighttime values. Sensitivity tests demonstrated that photo-enhanced NO_2 conversion on the ground could adequately explain P_{unknown}, while the nocturnal HONO production derived from soil emission fluxes (ranging from 0.32 ppbv h^{-1} to 0.79 ppbv h^{-1}) was sufficient to elucidate the nighttime P_{unknown}. Our study emphasized the variability of HONO fluxes across various agricultural management activities, as well as the importance of heterogeneous NO_2 conversion on the ground surface and soil emissions for HONO production.

1. Introduction

Nitrous acid (HONO) and nitrogen oxides (NO_x = NO + NO_2) are key components of reactive nitrogen (Nr) cycles and significantly influence the atmospheric oxidation capacity through the hydroxyl radical (OH) and ozone (O_3) atmospheric cycles (Kratz et al., 2022; Monks et al., 2009; Weber et al., 2015). The photolysis of HONO contributes to 20 %–90 % of the OH budget, serving not only as an important source of OH in the early morning but also playing a significant role throughout the entire day (Elshorbany et al., 2009; Kim et al., 2014; Kleffmann et al., 2005; Nan et al., 2017; Xue et al., 2020). Despite the significance of HONO in atmospheric chemistry, the formation mechanism of HONO is still not well understood, especially during the daytime. Unexpectedly large discrepancies have been found between HONO measurements and predicted values from known mechanisms, implying the existence of unknown sources of HONO that have not yet been identified (Lee et al., 2016; Liu et al., 2019c; Sörgel et al., 2011; Su et al., 2011; Tang et al., 2015). Several potential mechanisms have been proposed to explain atmospheric HONO levels, including direct emissions from combustion processes (Nakashima and Kajii, 2017; Nie et al., 2015); the chemical equilibrium between soil nitrite (NO_2^-) and hydrogen ions (Su et al., 2011); photosensitized reactions of NO_2 on organic substances (George et al., 2005), humic acids (Han et al., 2016; Stemmler et al., 2006), soot (Monge et al., 2010), minerals (Ndour et al., 2008), urban grime (Liu et al., 2019a), plant leaves (Marion et al., 2021), etc.; photolysis of adsorbed nitrates or nitric acid (Ye et al., 2017; Zhou et al., 2003; Zhou et al., 2011) and ortho-nitrophenols (Bejan et al., 2006; Guo and Li, 2022); direct emission from ammonia oxidizing bacteria and other microorganisms (Oswald et al., 2013; Scharko et al., 2015); desorption of adsorbed HONO from the surface by acid displacement processes (Vandenboer et al., 2013; Vandenboer et al., 2014; Vandenboer et al., 2015), and chemical reactions of hydroxylamine on the surface of soil particles (Ermel et al., 2018). Furthermore, the NH_3-promoted heterogeneous reaction of NO_2 has recently been proposed based on laboratory and field studies (Ge et al., 2019; Li et al., 2018; Xu et al., 2019), however, this mechanism and its atmospheric influences require further investigation.

Flux measurement is always considered as a useful tool for quantifying ground-level sources of HONO, providing direct insight into the production and loss processes on the surface. In recent years, micrometeorological methods such as relaxed eddy accumulation (REA) and aerodynamic gradient (AG) have been developed and applied in HONO flux research, with field observations primarily conducted in Europe and North America. Ren et al. (2011), Von Der Heyden et al. (2022) and Zhou et al. (2011)

measured HONO fluxes using the REA method in various environments such as agricultural fields, forests, and grasslands. The studies revealed that HONO fluxes were primarily driven by the photosensitized NO_2 reduction and photolysis of adsorbed HNO_3. Laufs et al. (2017), Meng et al. (2022) and Sörgel et al. (2015) performed measurements utilizing the AG method over bare soil, corn canopy, forest canopy, and wheat canopy, obtaining similar conclusions. Additionally, the chamber method provides greater flexibility and is suitable for multipoint observations within agricultural fields. Tang et al. (2020) and Xue et al. (2019) investigated HONO emissions from agricultural soil in the Huaihe River Basin and the North China Plain (NCP) by employing the open-top dynamic chamber method, confirming that agricultural soil emission is an important source of atmospheric HONO. However, the limited available HONO flux studies indicated different potential HONO precursors, which demonstrated the necessity for more HONO flux measurements to explore potential HONO formation pathways. Moreover, most flux measurements are typically conducted for the short term (less than one month), and cannot cover the entire growing season of crop. Research on HONO fluxes in agriculture has primarily focused on wheat–maize rotations and the effects of fertilization. Paddy fields, as a major crop in southern China with unique growth conditions, have received little attention, resulting in limitations in understanding the Nr budget in paddy field ecosystems.

Cropland, which covers 50 % of the global habitable areas (FAO, 2022), plays a crucial role in the global nitrogen budget. The application of nitrogen fertilizers has been instrumental in boosting food production. Nevertheless, the overuse of fertilizers has also resulted in soil degradation, declining air quality, and adverse effects on human health. Simultaneously, the extensive application of synthetic nitrogen fertilizers in cropland, coupled with their low nitrogen use efficiency (< 50 % on average) (Mueller et al., 2017; Zhang et al., 2015), has led to the release of excess Nr from the soil through microbial processes. Among these, NO_x mediates the production and destruction of O_3, influences the formation of the OH radical, and can be oxidized to nitric acid and nitrate, thereby increasing wet and dry nitrogen deposition in ecosystems (Pilegaard, 2013). Notably, the positive effect of nitrogen fertilizer on HONO emissions has been consistently verified (Wang et al., 2021). Xue et al. (2019) reported an extraordinarily high HONO flux of 1515 ng N m^{-2} s^{-1} under excessive fertilized conditions, which greatly exceeded the emissions from unfertilized farmland and even surpassed laboratory results. This underscores the significant potential for Nr emissions originating from agricultural soil. Therefore, it is imperative to comprehend the fluxes within agricultural ecosystems to elucidate the mechanisms of Nr production and loss. The lack of field data on HONO fluxes in paddy fields, coupled with the ambiguous impacts of agricultural management activities, hinders our understanding of soil–atmosphere exchange mechanisms. Laboratory studies have also demonstrated HONO and NO emissions at high water content (Wang et al., 2021; Wu et al., 2019), and the anaerobic denitrification in oxygen-limited environments can be an important source of HONO (Bhattarai et al., 2021; Wang et al., 2021; Wu et al., 2019). This highlights the necessity to investigate further the effects of flooded paddy fields and agricultural practices on soil HONO emissions.

In this study, the soil–atmosphere exchange processes were investigated using the AG method in conjunction with the BroadBand Cavity Enhanced Absorption Spectrometer (BBCEAS) system and NO_x analyzer in paddy fields located in the Huaihe River Basin. The variations in HONO and NO_x levels and fluxes were evaluated across various agricultural management processes from June to July, corresponding to the paddy growing season. Additionally, a particular focus was placed on investigating the sources of HONO during the rotary tillage period and its contribution to atmospheric oxidizing capacity.

2. Materials and methods

2.1 Measurement site

The field campaign was performed at the Shouxian National Climatological Observatory (32°25′ N, 116°47′ E; 25 m above sea level), located 9 km south of Shouxian, Anhui Province (Fig. S1). This location represents a typical rice–wheat rotation ecosystem in the Huang–Huai agro-ecological region, which serves as the primary grain production area in China, contributing to 18 % of the nation’s total grain production. Additionally, it is responsible for 76.3 % of the country’s total nitrogen fertilizer application (Cao et al., 2019). The site covers a 17 ha field and is dedicated to the cultivation of rice–wheat rotation. It serves as an experimental site for studying surface–atmosphere exchange. The site is situated amidst other agricultural fields, with a less traffic road to the north (250 m). The prevailing climate in the region is subtropical monsoon, characterized by distinct seasons, with high temperatures and rainfall occurring in the same season. The average annual temperature is 14.8 °C, and the average annual precipitation is 905 mm.

2.2 Experimental design

The flux measurement was conducted from 1 June to 14 July 2021, immediately following the winter wheat harvest on 31 May 2021. The tillage process took place over 11 days from 2 June to 13

June, followed by flooding irrigation, and fertilization with compound fertilizer (N–P_2O_5–K_2O 15 %–15 %–15 %) of 67.5 kg N ha^{-1} before 22 June 2021. Consequently, the surface was a mixture of bare soil and sparse winter wheat residues before irrigation (June 13th, 9:00), while the soil became waterlogged after flooding irrigation. The paddy seedlings were transplanted on 26 and 27 June at a density of 1.8×10^5 plants ha^{-1}, growing from 0.14 m to approximately 0.22 m during the whole campaign. Additionally, irrigation was employed post-paddy transplantation to mitigate water deficiency during the growth phase, thereby preventing the potential mortality of paddy seedlings. The 46 %–N urea solution of 69 kg N ha^{-1} was applied as top-dressing on 10 July.

The concentrations of HONO and NO_2 in the ambient air were measured using a homemade BBCEAS instrument with a time resolution of 1 min and detection limits of 54 pptv (2σ) for HONO and 98 pptv (2σ) for NO_2. The measurement uncertainty was 8.7 % and 8.1 % for HONO and NO_2, respectively. Further details regarding BBCEAS, such as its principle, instrument parameters and quality control, are described in detail elsewhere (Duan et al., 2018; Tang et al., 2019). NO was measured by custom-built chemiluminescence (Model 42iTL, Thermo Scientific, USA), and O_3 were measured with Thermo Scientific Model 49i, with detection limits of 50 pptv for NO and 500 pptv for O_3, respectively. The measurement of soil temperature and moisture, as well as meteorological and micrometeorological parameters, are presented in Text S1.

Trace gas profiles of HONO, NO, and NO_2 were obtained using inlets positioned at heights of 0.2 m and 1.6 m, which were adjusted to 0.3 m and 1.6 m on 27 June to accommodate the canopy height, consistently exceeding the canopy height throughout the campaign (Fig. 1). Two BBCEAS instruments were used to measure HONO and NO_2 at different heights, which were intercompared several times throughout the campaign and exhibited excellent agreement (HONO: $R^2 = 0.989$; NO_2: $R^2 = 0.998$) with slopes close to 1 (Fig. S2). A NO_x analyzer for NO measurement was connected to a Teflon solenoid valve to allow sequential measurements at two different heights. All instruments were placed in the thermostated container controlled by an air conditioner, with the external sampling inlets affixed to a small mast. The sampling inlets were oriented away from the mast towards the prevailing wind direction to minimize turbulence disruption. To prevent photolysis and the condensation of water vapor, the PFA inlet lines (7.5 m length with a 6 mm external diameter) were shielded from radiation and slightly heated with heating tape (the heating temperature was about 30 °C).

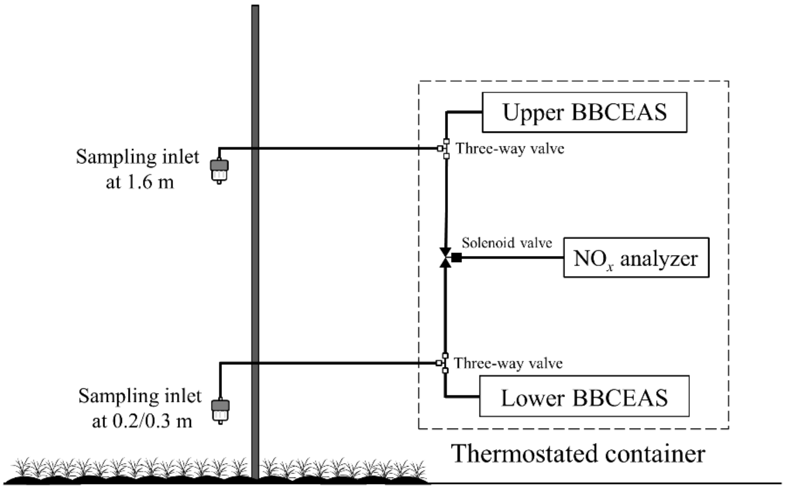

Figure 1. The aerodynamic gradient measurement set-up for the determination of HONO, NO and NO_2 fluxes.

2.3 Aerodynamic gradient fluxes of HONO, NO and NO_2

The HONO, NO and NO_2 fluxes were calculated by the AG method at time intervals of 30 min, which has been elaborated upon in previous studies (Laufs et al., 2017; Meng et al., 2022; Stella et al., 2012) and will be briefly introduced here. The flux (F_χ) of trace gas is calculated from the friction velocity (u_*) and the mixing ratio scaling parameter (χ_*) as follows:

$$F_\chi = -u_*\chi_* \tag{1}$$

where u_* is calculated from eddy covariance measurements and χ_* is defined from stability-corrected gradient of the scalar mixing ratio (χ) with height (z) as:

$$\chi_* = \kappa \cdot \frac{\partial\chi}{\partial\left[\ln(z-d)-\Psi_{\mathrm{H}}\left(\frac{z-d}{L}\right)\right]} \tag{2}$$

The fluxes ($F_{\mathrm{HONO,NO\ and\ NO_2}}$) of trace gases at geometric mean height can be expressed as:

$$F_{\mathrm{HONO,\ NO\ and\ NO_2}} = -\kappa \cdot u_* \cdot \frac{\partial c(\mathrm{HONO,\ NO\ and\ NO_2})}{\partial\left[\ln(z-d)-\Psi_{\mathrm{H}}\left(\frac{z-d}{L}\right)\right]} \tag{3}$$

where κ is von Kármán constant (κ = 0.4), z is the height above the ground, d is zero plane displacement and was taken as $2/3 \cdot h_c$ (h_c is the canopy height), L is the Obukhov length and Ψ_{H} is integrated stability correction function for scalars (Sutton et al., 1993).

Data from all instruments could not always be collected simultaneously for flux calculation due to various factors such as calibration, malfunction, and disturbances from agricultural activities. Consequently, the affected data were excluded when calculating fluxes. The dataset used for the determination of HONO, NO and NO_2 fluxes comprised 68 % for HONO, 81 % for NO, and 86 % for NO_2. The total uncertainty in the flux is composed of gradient error and friction velocity error (Laufs et al., 2017; Meng et al., 2022). The average uncertainty for HONO, NO, and NO_2 fluxes were 11 %, 16 %, and 20 % (median [25 percentile–75 percentile]), respectively. Furthermore, the fluxes were discarded for very stable conditions with low wind speed and friction velocity. It is important to note that HONO, NO and NO_2 are subject to chemical reactions, which could lead to a vertical divergence of flux between the surface and the measurement height. The influence of chemical reactions during turbulent transport was checked utilizing the Damköhler number (*DA*), as detailed in Text S2. The divergence by chemical reactions of HONO could be neglected when interpreting the potential sources of HONO and driving factors of HONO flux. The *DA* for the NO-O_3-NO_2 triad generally exhibited values less than 1, however, a sharp increase in flux divergence occurred when the *DA* became greater than 1 (Stella et al., 2012). Additionally, the upward NO_2 flux exhibited a significant correlation ($R = 0.82$) with NO flux, suggesting that the upward NO_2 fluxes could be attributed to the reaction of NO and O_3. Consequently, in light of the influence of chemical reactions on the fluxes of NO and NO_2, these fluxes (5.9 % for NO flux and 10.5 % for NO_2 flux) were excluded from subsequent analysis.

3. Results and discussion

3.1 Overview of meteorological and soil parameters

The time series of meteorological parameters throughout the observation period is shown in Fig. 2. The campaign weather was dominated by sunny days, with 64 % of the days having a daily maximum global radiation above 700 W m^{-2}. The ambient temperature and soil temperature ranged from 17.0 to 36.6 °C and 20.0 to 34.8 °C, with average values of 26.8 ± 3.5 °C and 26.5 ± 2.7 °C, respectively. The relative humidity (RH) and soil water-filled pore space (WFPS) ranged from 22 % to 98 % and 44 % to 88 %, with average values of 77 % ± 17 % and 69 % ± 15 %, respectively. The average wind speed was 3 m s^{-1}, with a maximum wind speed of 11.0 m s^{-1} occurring during the rotary tillage period. The $PM_{2.5}$ concentration varied from 1 to 100 μg m^{-3}, with its daily average value remaining below the Chinese National Ambient Air Quality Standard (Class II: 75 μg m^{-3}). Intermittent rainfall occurred from June 13 to July 5, with a total precipitation of 186.1 millimeters. Notably, after irrigation in the agricultural field on June 13, WFPS increased from 45 % to 80 %.

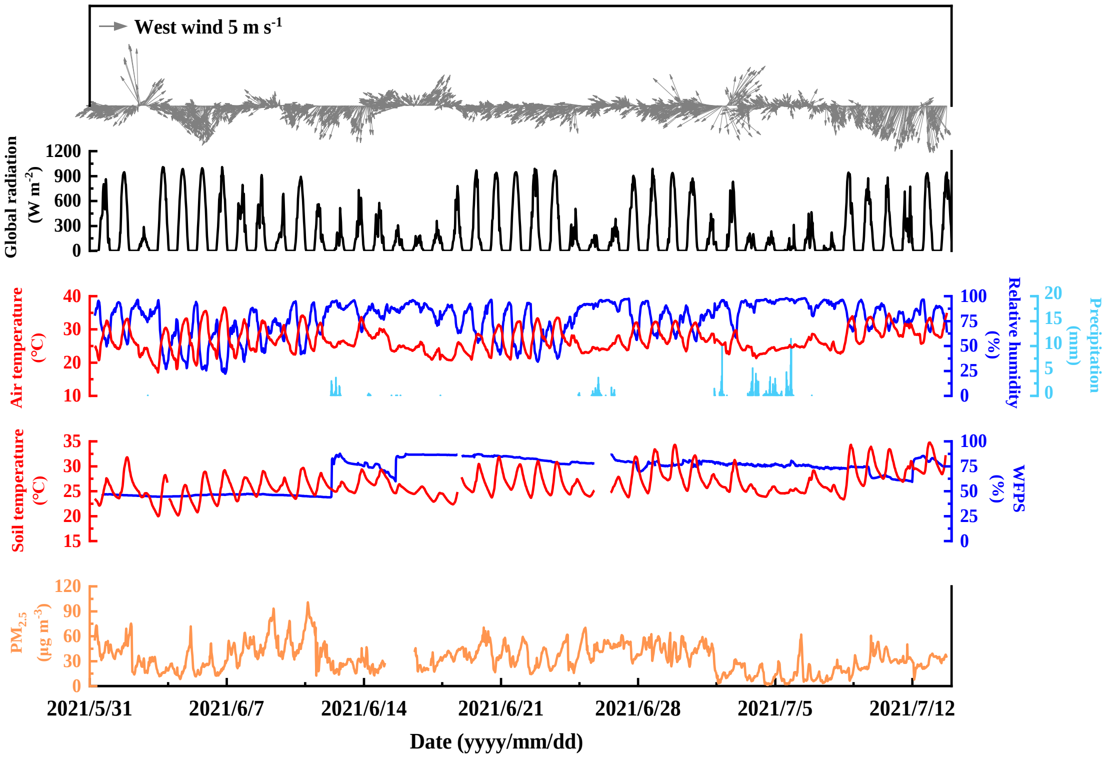

Figure 2. Temporal variations of meteorological parameters (wind speed and direction, air temperature, relative humidity and precipitation), soil temperature, WFPS and $PM_{2.5}$ measured from 1 June to 14 July 2021.

3.2 Mixing ratio differences and fluxes of HONO, NO and NO_2

The field campaign was performed across various agricultural management activities, including rotary tillage (June 2–13), flooding irrigation (June 13–19), fertilization (June 19–21), paddy cultivation (June 26–27), and top-dressing (July 10). Figure 3 illustrates the time series of HONO, NO, NO_2 and O_3 mixing ratios. Throughout the campaign, the ambient O_3 concentrations varied from 0.54 to 131.57 ppbv, with an average of 48.44 ± 26.29 ppbv. The peak of NO mixing ratios reached 36.02 ppbv during rotary tillage, and the average mixing ratios of NO at lower (0.2/0.3 m) and upper levels (1.6 m) were 0.75 ± 2.21 ppbv and 0.46 ± 1.16 ppbv, respectively. Higher NO mixing ratios were measured at the lower level, likely due to soil NO emissions caused by microbiological activity (Bargsten et al., 2010; Ludwig et al., 2001). Moreover, the average NO_2 mixing ratios were 4.48 ± 4.96 ppbv and 4.75 ± 4.38 ppbv at lower and upper levels, respectively. The synchronous peaks of NO and NO_2 and the decrease of O_3 (e.g. in the early hours of June 7) indicated that NO release from soil could react rapidly with O_3 to form NO_2. The ambient HONO mixing ratios ranged from below detection limits to 3.60 ppbv at the lower level and 2.36 ppbv at the upper level, with an average of 0.46 ± 0.59 ppbv and 0.37 ± 0.37 ppbv, respectively. The average $HONO/NO_x$ ratio of 0.079 ± 0.059 was significantly higher than the range for direct emissions from vehicle exhaust reported in previous studies (0.003–0.018) (Kirchstetter et al., 1996; Kurtenbach et al., 2001; Liang et al., 2017; Liu et al., 2017; Nakashima and Kajii, 2017; Nakashima and Kondo, 2022), and was comparable to the value (0.0929) observed in summer agricultural fields in the NCP (Song et al., 2022). Notably, successive HONO peaks were measured during rotary tillage, with HONO mixing ratios reaching 3.60 ppbv at the lower level. These values exceeded those observed during the winter at the same site (Meng et al., 2022) and were comparable to observations at suburban sites in the Pearl River Delta (Li et al., 2012; Su et al., 2008) and rural sites in the NCP (Xue et al., 2020). However, HONO levels declined rapidly following flooding irrigation (see Fig. 3 and Table 1). Subsequent to the fertilization and the top-dressing, a noticeable rise in HONO levels was observed, which could be attributed to the increase in HONO release by fertilizer application at high water contents (Tang et al., 2019; Wang et al., 2021; Wu et al., 2019; Xue et al., 2019). Nevertheless, these levels were significantly lower than the mixing ratios observed during rotary tillage.

Table 1. The statistical summary of HONO, NO, NO_2, HONO flux, NO flux and NO_2 flux across various agricultural activities spanning from 1 June to 14 July 2021.

Agricultural activities		HONO (ppbv)		NO (ppbv)		NO_2 (ppbv)		HONO flux (nmol m^{-2} s^{-1})	NO flux (nmol m^{-2} s^{-1})	NO_2 flux (nmol m^{-2} s^{-1})
		0.2/0.3 m	1.6 m	0.2/0.3 m	1.6 m	0.2/0.3 m	1.6 m			
Rotary tillage	Ave	0.99	0.69	1.88	0.87	6.26	6.56	0.26	0.47	-0.72
	Min	0.08	0.07	0.07	0.06	0.70	0.90	-0.62	-0.78	-3.50
	Max	3.60	2.36	36.02	17.80	22.24	35.03	1.86	9.12	0.29
Flood irrigation	Ave	0.19	0.18	0.66	0.46	4.62	4.91	0.02	0.18	-0.40
	Min	0.04	0.06	0.13	0.08	1.11	1.11	-0.40	-0.78	-1.93
	Max	0.52	0.44	9.22	2.12	17.31	19.92	0.32	1.18	0.50
Fertilization	Ave	0.24	0.31	0.33	0.28	5.81	6.15	-0.06	0.03	-0.34
	Min	0.08	0.07	0.06	0.05	0.39	0.64	-0.38	-0.13	-1.37
	Max	0.61	0.71	7.02	4.14	30.30	29.07	0.11	0.31	0.07
After fertilization	Ave	0.30	0.36	0.26	0.26	4.58	4.49	-0.05	0.001	-0.19
	Min	0.06	0.05	0.05	0.06	0.69	0.88	-0.41	-0.23	-1.17
	Max	1.05	1.29	4.09	4.61	19.25	20.32	0.26	0.12	0.26
Paddy cultivation and growth	Ave	0.18	0.21	0.42	0.39	3.45	3.76	-0.05	0.02	-0.34
	Min	0.04	0.05	0.05	0.05	0.29	0.53	-0.70	-1.01	-1.93
	Max	0.63	0.69	15.21	12.40	14.32	15.85	0.42	0.44	0.50
Top-dressing	Ave	0.23	0.19	0.24	0.22	2.78	3.02	0.05	0.03	-0.29
	Min	0.05	0.05	0.05	0.05	0.49	0.63	-0.34	-0.37	-3.26
	Max	1.21	0.51	1.57	1.31	9.59	9.49	0.57	1.27	0.09

Note: Ave, Min, and Max represent the average, minimum, and maximum, respectively. The 0.2/0.3 m and 1.6 m represented the lower and upper levels, respectively.

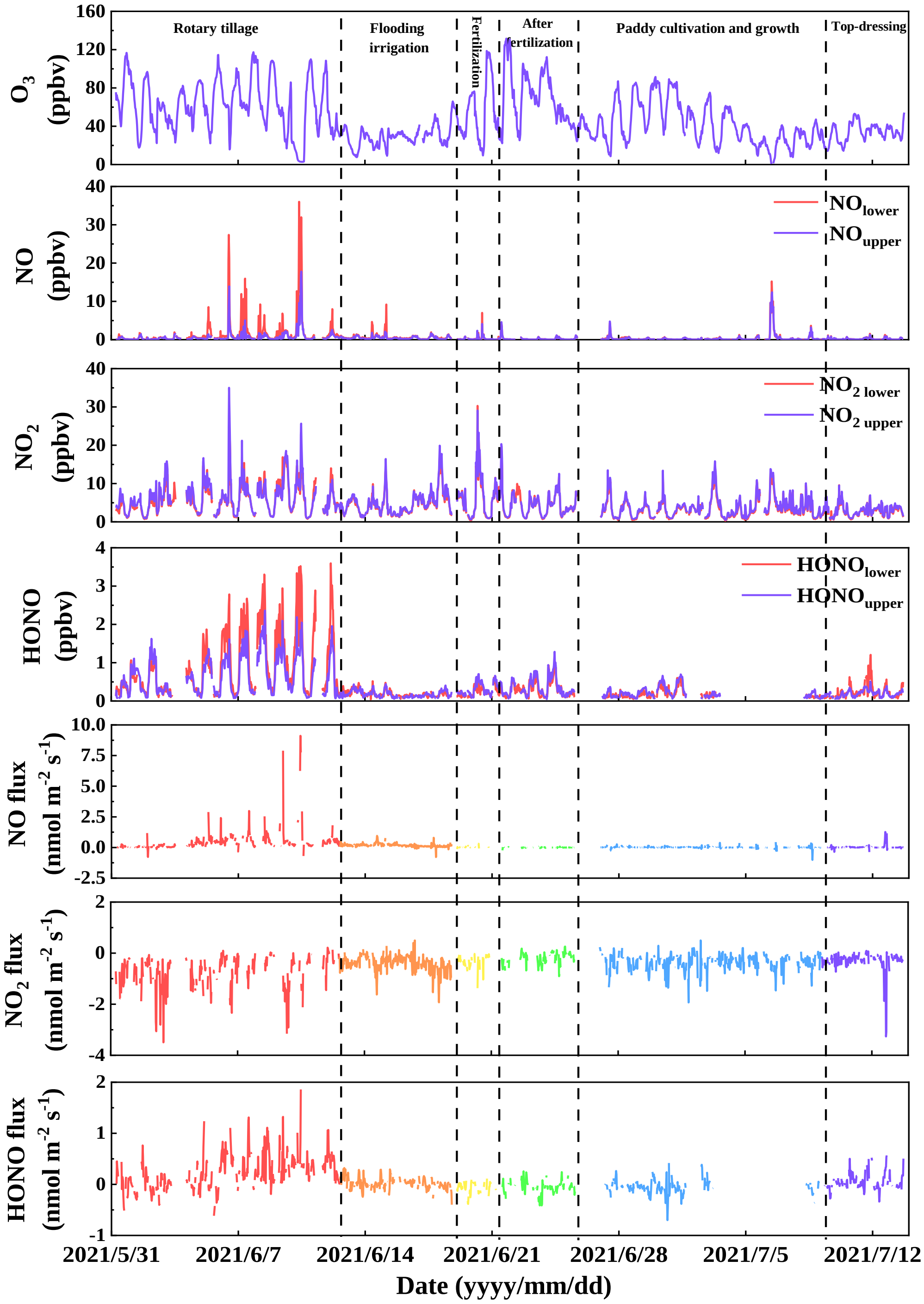

Figure 3. Time series of O_3, NO, NO_2, HONO and the fluxes of HONO, NO, and NO_2 were determined by the aerodynamic gradient method. The mixing ratios of HONO, NO, NO_2 (lower level: 0.2/0.3 m, upper level: 1.6 m), and O_3 were measured above a crop rotation field and averaged for 30 min intervals. Periods of agricultural management activities (rotary tillage, flood irrigation, fertilization, after fertilization, paddy cultivation and growth, top-dressing) are denoted at the top of the graph.

The fluxes of HONO, NO, and NO_2 determined by the AG method are illustrated in Fig. 3. Upward fluxes were commonly observed for HONO and NO, while NO_2 was deposited to the ground. The magnitudes of observed HONO fluxes ranged from -0.70 to 1.86 nmol m^{-2} s^{-1}, with an average of 0.07 ± 0.22 nmol m^{-2} s^{-1}, which falls within the range of the HONO flux measurements in rural and suburban regions from the literature (see Table 2). The upward HONO fluxes were mostly observed during rotary tillage, reaching up to 1.86 nmol m^{-2} s^{-1}. After the irrigation, the increase in soil moisture content (~80 % WFPS) led to a significant reduction in HONO flux. Previous laboratory studies have also demonstrated that lower levels of HONO flux at high water holding capacity, low gas diffusion rates and high solubility could limit the release of HONO from soil (Ermel et al., 2018; Meusel et al., 2018; Wu et al., 2014). The observations before and after irrigation demonstrate the regulatory role of soil moisture in the HONO exchange process, which has been systematically investigated by examining HONO emission flux as a function of soil moisture in previous studies (Mamtimin et al., 2016; Wang et al., 2021). Soil moisture determines whether nitrification or denitrification processes dominate gas emissions and strongly influences the corresponding gas emission rates and concentration compensation points (Cheng, 2013). Several laboratory findings indicate that nitrification under low soil moisture conditions is the dominant process for HONO emissions (Oswald et al., 2013; Scharko et al., 2015), and field observations of HONO have predominantly focused on dryland ecosystems (Ren et al., 2011). Conversely, Wu et al. (2019) demonstrated that soil under high water content (75 %–140 % WHC) can also exhibit substantial emissions of HONO, with an average ratio of the highest HONO flux of wet peak to dry peak being approximately 30 %. However, actual field observations have revealed that HONO fluxes are very low (close to 0) under high water content conditions, which may be attributed to the influence of soil moisture on microbial metabolic activity and gas diffusion in the soil (Hu et al., 2015; Linn and Doran, 1984). Furthermore, Wang et al. (2021) reported the promoting effect of fertilization on HONO flux under high soil moisture conditions (75 %–95 % WHC). Nevertheless, we did not observe this phenomenon in our field experiments with paddy fields. This discrepancy could probably be attributed to the anaerobic or microaerobic conditions created by pre-fertilization irrigation, which exerted a greater inhibitory effect on the nitrification process than the promoting effect of fertilization. Currently, the estimation of HONO flux at the regional scale relies more on laboratory research findings (Gan et al., 2024; Wu et al., 2022). This study highlights discrepancies between laboratory and field observations within the high soil water content range, which pose significant challenges to the uncertainty of estimation results.

The agricultural field acted as a well-known source of atmospheric NO, with an average flux of 0.19 ± 0.53 nmol m^{-2} s^{-1} in this study. Similar to HONO, the upward NO flux was mostly observed during rotary tillage, with a maximum flux of 9.12 nmol m^{-2} s^{-1} in the early morning (Table 1). This finding is consistent with previous studies exhibiting that tillage increases NO emission (Chatskikh and Olesen, 2007; Fang et al., 2006; Fang and Yujing, 2009; Liu et al., 2005; Pinto et al., 2004; Sehy et al., 2003; Yao et al., 2009; Yamulki and Jarvis, 2002). However, the NO fluxes were close to zero when the paddy field was waterlogged, probably because the nitrification process that dominates NO production in soil was greatly hindered in water-saturated soil and anoxic microsites (Fang and Yujing, 2009). Similarly, we also did not observe significant emissions of HONO under sustained high moisture conditions. The coincidences of peaks in HONO flux and NO flux during rotary tillage suggest that HONO release from soil, similar to NO, is associated with microbial activity in soil (Bargsten et al., 2010; Skiba et al., 1993). Furthermore, the notably elevated fluxes of HONO and NO were observed during rotary tillage in comparison to other phases of agricultural activities (Fig. S3). The higher emission rates of NO and HONO could account for the successive peaks in their concentrations and fluxes. Similar to NO, the emission of HONO from soil could be significantly stimulated by soil tillage. Besides, the average NO_2 flux of -0.42 ± 0.44 nmol m^{-2} s^{-1} (ranging from -3.50 to 0.50 nmol m^{-2} s^{-1}) indicated that the agricultural field acted as a sink for atmospheric NO_2 (Fang and Yujing, 2009; Tang et al., 2020).

Table 2 Summary of the maximum and minimum of HONO flux in field measurements over different soil types at remote/rural/suburban sites.

Soil type	Method	HONO flux[a] (nmol m^{-2} s^{-1})		HONO flux[b] (nmol m^{-2} s^{-1})		Reference
		Min	Max	Min	Max	
Grassland	AG	-0.09	0.53	–	–	Harrison and Kitto (1994)
		-0.21	0.70			
Forest	AG	0.02	0.07	–	–	Sörgel et al. (2015)
Maize	AG	–	–	0.01	0.16	Laufs et al. (2017)
Wheat	AG	-0.39	1.10	-0.003	0.20	Meng et al. (2022)
Agricultural field	REA	-0.30	0.50	-0.007	0.10	Ren et al. (2011)
Forest	REA	-0.50	1.31	0.03	0.19	Zhou et al. (2011)
Forest	REA	0.03	0.19	–	–	Zhang et al. (2012)

Grassland	REA	-0.06	0.16	0.02	0.07	Von Der Heyden et al. (2022)
		0.04	0.23	–	–	
Maize	OTDC	0.41	2.89	–	–	Xue et al. (2019)
		–	108.21	–	–	
Maize	OTDC	–	2.84	-0.06	1.45	Tang et al. (2019)
Wheat	OTDC	-0.09	0.55	–	–	Tang et al. (2020)
Maize	OTDC	-0.61	22.79	0.01	10.86	Song et al. (2023)
		–	0.33	–	–	
Maize	OTDC	–	11.50	–	–	Xue et al. (2024)
		–	24.86	–	–	
Paddy	AG	-0.70	1.86	0.01	0.15	This study

AG: aerodynamic gradient; REA: relaxed eddy accumulation; OTDC: open-top dynamic chamber; HONO flux^a: values in the time series; HONO flux^b: values in the diurnal variations;

3.3 Diurnal profiles of fluxes and HONO source during rotary tillage

The diurnal variations of NO_2 photolysis frequency ($J(NO_2)$), air temperature, relative humidity, soil temperature, WFPS, NO flux, NO_2 flux, and HONO flux are illustrated in Fig. 4. The diurnal HONO flux exhibited no discernible diurnal pattern during the whole campaign, which was similar to the diurnal profile observed during BEARPEX 2009 in California (Ren et al., 2011). Significant HONO emissions were primarily observed during rotary tillage, and its daily pattern is depicted in Fig. 4. Upward HONO fluxes were observed throughout the day, with a maximum value of 0.55 nmol m^{-2} s^{-1} in the early morning. The distinct HONO emissions were observed in the morning after sunrise. Moreover, the magnitudes of the daytime fluxes (0.25 ± 0.13 nmol m^{-2} s^{-1}) were comparable to the nocturnal values (0.27 ± 0.13 nmol m^{-2} s^{-1}). The diurnal profile of NO flux exhibited consistent levels of NO emission throughout the day, except for a noticeable peak in the early morning. It is worth noting that the synchronous peak of HONO flux and NO flux was observed in the morning. In contrast to the fluxes of HONO and NO, deposition was the prevailing process for NO_2 flux. A greater downward NO_2 flux of -0.85 ± 0.27 nmol m^{-2} s^{-1} (-0.57 ± 0.23 nmol m^{-2} s^{-1} at night) was observed during the daytime, potentially due to an increase in the dry deposition velocity of NO_2 during the day.

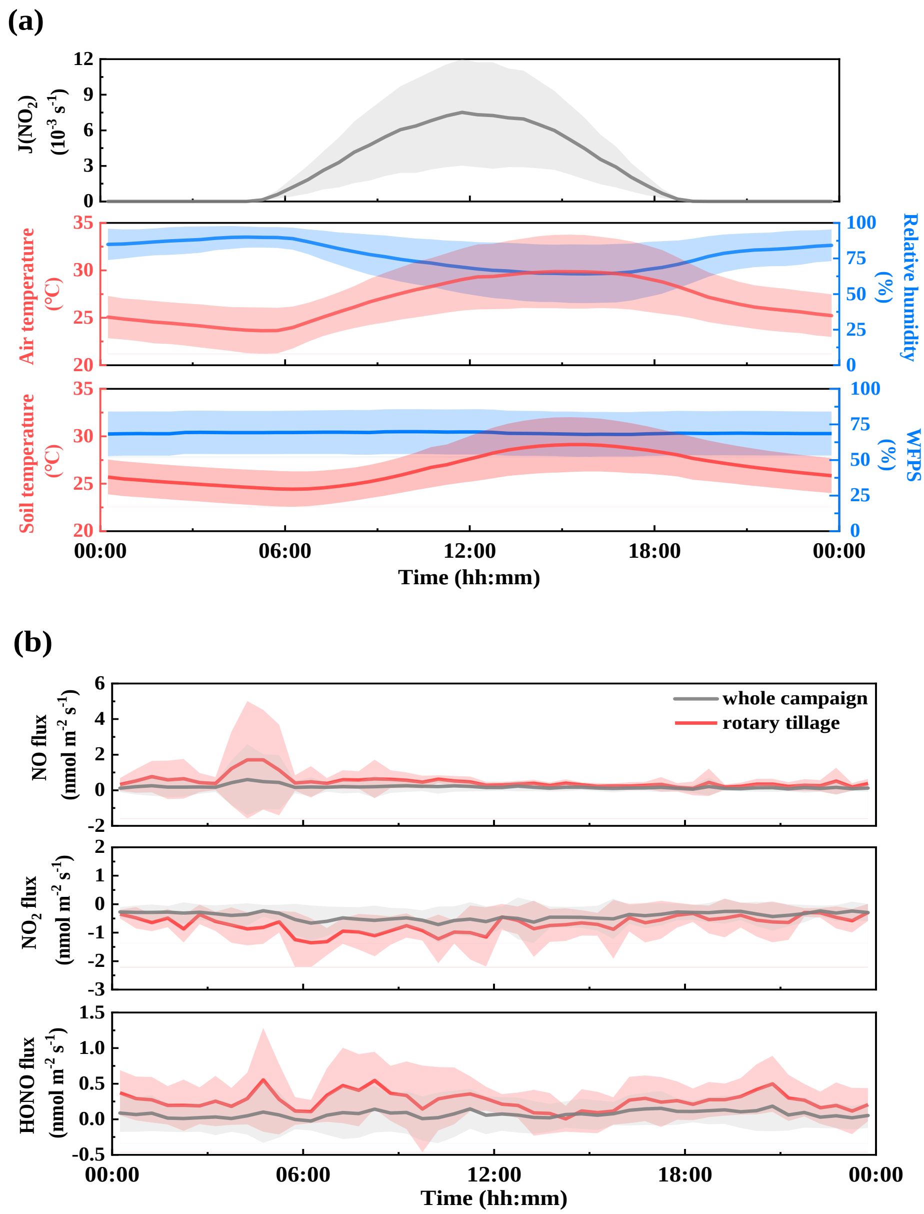

Figure 4. (a) Diurnal variations of NO_2 photolysis frequency ($J(NO_2)$), air temperature, relative humidity, soil temperature and WFPS throughout the whole campaign. (b) Diurnal profiles of HONO, NO and NO_2 fluxes are presented for the whole campaign and rotary tillage. The error bars denoted the standard deviation.

Throughout the rotary tillage period, the emissions of HONO and NO were significant, with the maximum fluxes reaching 1.86 nmol m^{-2} s^{-1} for HONO and 9.12 nmol m^{-2} s^{-1} for NO. The concurrent peaks in HONO and NO fluxes indicate that HONO emissions could originate from soil sources, as it is well-established that NO is primarily generated and released from soil microbial processes (Feig et al., 2008; Rende et al., 1989). As shown in Fig. 5, a significant correlation ($R = 0.77$) was observed between the fluxes of HONO and NO during the rotary tillage period, suggesting a shared source for both gases. This could be attributed to the generation and release from soil microbial processes, aligning with the results reported by Tang et al. (2020). A gaussian fitting was employed to analyze the variation of HONO and NO fluxes with soil temperature (Fig. S4). It was found that both HONO and NO exhibited maximum emission fluxes at approximately 25 °C and 24 °C, respectively, which is close to the optimal temperature (25 °C) for soil microbial nitrification and denitrification processes (Agehara and Warncke, 2005; Fang and Yujing, 2009). This finding further supports the hypothesis that HONO is generated and released from soil biological processes. Additionally, there was an indication of elevation in HONO flux during periods of intense solar radiation in the morning. Although the correlations of HONO flux with NO_2, $J(NO_2)$ and NO_2 flux were found to be low (R = 0.28, 0.12 and 0.25), we observed a significant correlation (R = 0.60) between HONO flux and the product of $J(NO_2)$ × NO_2 (Fig. 6), as well as a moderate correlation (R = 0.41) with the product of $J(NO_2)$ × NO_2 flux (Fig. S5). This indicates that the light-induced NO_2 conversion serves as an important source of HONO during the day. Furthermore, another mechanism of acid displacement can be ruled out, as the major strong acid, HNO_3, is primarily generated during the daytime and subsequently deposited to the ground. Consequently, the peak of the HONO source is expected to occur in the afternoon (Vandenboer et al., 2015). Finally, the results indicate that both mechanisms of soil release from biological processes and light-induced NO_2 conversion are likely active, which together affect the diurnal HONO flux pattern.

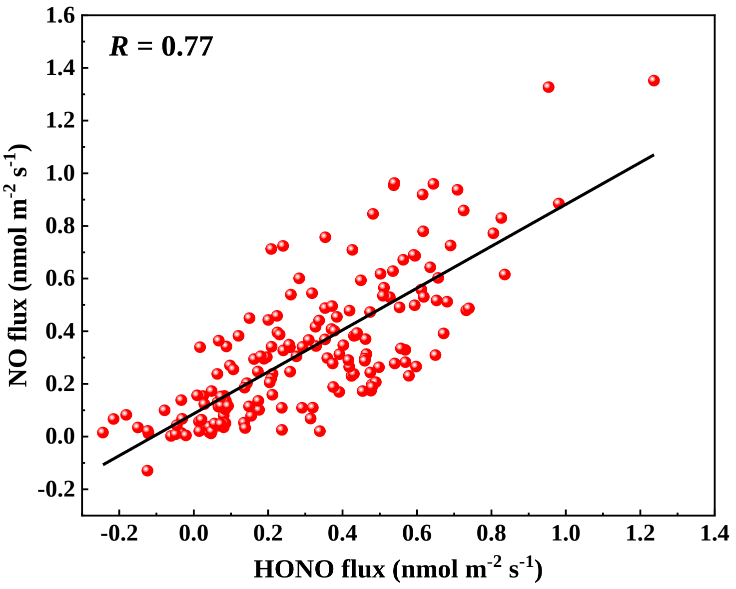

Figure 5. Correlation of HONO flux with NO flux during rotary tillage.

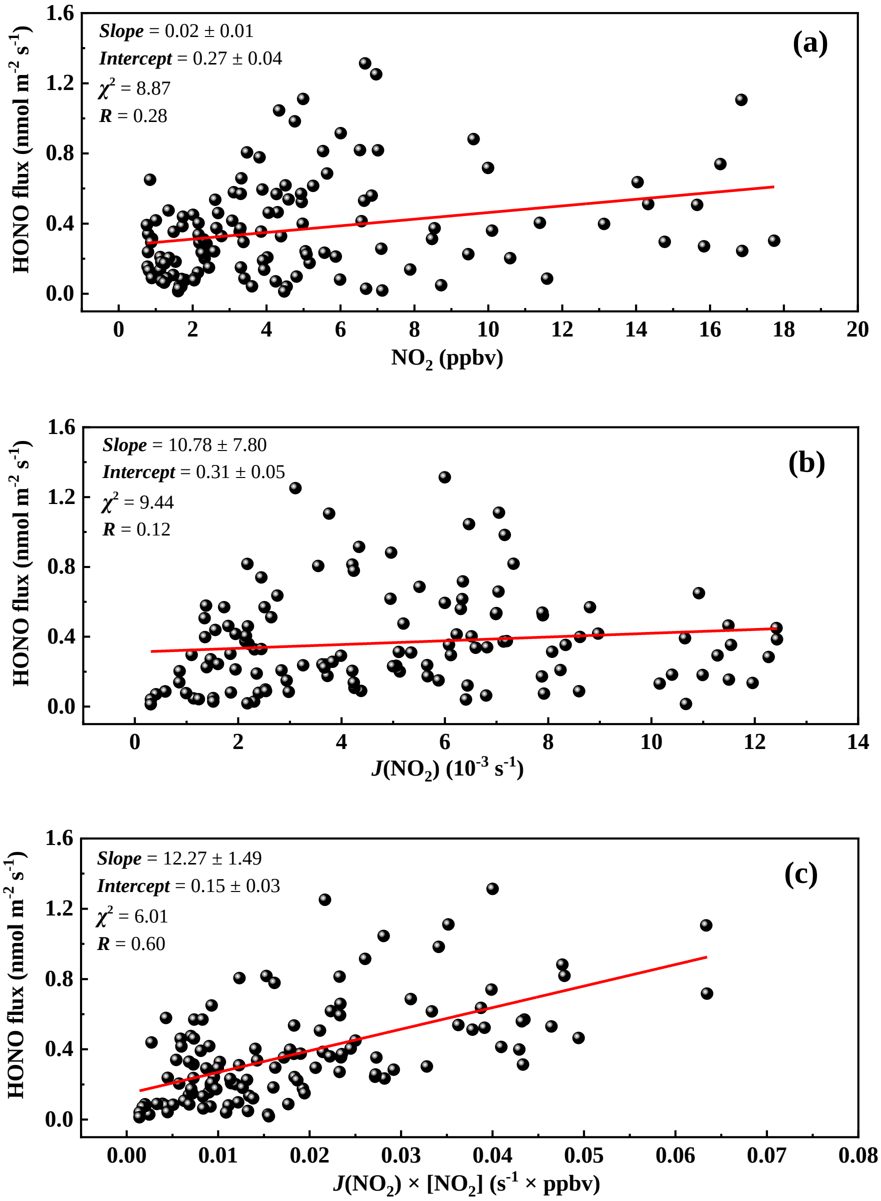

Figure 6. Correlation of the daytime HONO flux with (a) NO_2, (b) $J(NO_2)$ and (c) the product of $J(NO_2) \times [NO_2]$ during rotary tillage.

3.4 HONO budget during rotary tillage

In Section 3.3, we presented the potential sources of HONO flux during rotary tillage by conducting correlation analysis. Here, we will further calculate the specific contributions of HONO sources through budget analysis. The HONO budget can be derived from known HONO sources and sinks, and the potential unknown HONO source during rotary tillage was estimated. The lower-level data that better describe ground source processes were used for budget analysis. In this study, the investigated HONO sources including homogeneous reaction ($P_{\mathrm{OH+NO}}$), heterogeneous reaction of NO_2 on the aerosol surface and the ground surface (P_{aerosol} and P_{ground}). The HONO sinks included the reaction of HONO with OH

($L_{\mathrm{OH+HONO}}$), photolysis of HONO (L_{photo}) and dry deposition loss of HONO (L_{dep}). The calculation of HONO sources and sinks, as well as the estimates of the mixing layer height (MLH) is described in detail in Text S3 in the Supplemental Material.

$$\frac{d\mathrm{HONO}}{dt} = \left(P_{\mathrm{OH+NO}} + P_{\mathrm{unknown}} + P_{\mathrm{aerosol}} + P_{\mathrm{ground}}\right) - \left(L_{\mathrm{OH+HONO}} + L_{\mathrm{photo}} + L_{\mathrm{dep}}\right) \quad (4)$$

Simplifying Eq. (4), the $d\mathrm{HONO}/dt$ is approximated by $\triangle\mathrm{HONO}/\triangle t$. Then Eq. (4) is turned to Eq. (5):

$$P_{\mathrm{unknown}} = \frac{\triangle\mathrm{HONO}}{\Delta t} + L_{\mathrm{OH+HONO}} + L_{\mathrm{photo}} + L_{\mathrm{dep}} - P_{\mathrm{OH+NO}} - P_{\mathrm{aerosol}} - P_{\mathrm{ground}} \quad (5)$$

The average production and loss rates for the diurnal HONO budget are shown in Fig. 7. The homogeneous reaction of NO and OH accounted for 12.8 % of HONO production, and an average of $P_{\mathrm{OH+NO}}$ was 0.15 ± 0.10 ppbv h^{-1}. The heterogeneous conversion of NO_2 on the ground surfaces accounted for 12.4 % (0.1 ± 0.07 ppbv h^{-1}) of HONO production at night. P_{aerosol} (0.01 ± 0.006 ppbv h^{-1}) was negligible compared to other HONO sources due to its relatively small aerosol surface area (Fig. S6). The photodecomposition (L_{photo}) was the primary sink of HONO during the daytime, with a peak of 2.03 ppbv h^{-1} at 11:00 and an average of 1.44 ± 0.69 ppbv h^{-1}, while $L_{\mathrm{OH+HONO}}$ was very small and less than 5 % of L_{photo}. The dry deposition of HONO (L_{dep}) was influenced by the mixing layer height (MLH) and dominated the loss of HONO at night, with a rate exceeding 0.6 ppbv h^{-1}. P_{unknown} exhibited the obvious diurnal variation, with higher values during daytime (1.31 ± 0.54 ppbv h^{-1}) and lower values at night (0.53 ± 0.25 ppbv h^{-1}). The peak of P_{unknown} occurred during 7:00–12:00, with a maximum value of 2.18 ppb h^{-1}. The peak value of P_{unknown} is comparable to that measured in Taizhou (2.5 ppbv h^{-1}) (Ye et al., 2023) and larger than in Wangdu (0.62 ppbv h^{-1}) (Song et al., 2022), Nanjing (1.04 ppbv h^{-1}) (Liu et al., 2019b). Similar to the observed asymmetry around noon reported in previous studies, this could be attributed to the combined effect of solar radiation and the variation of precursor NO_2 (Song et al., 2022; Xue et al., 2022). As the significantly larger unknown source strength of HONO during the daytime, we focused on analyzing the unknown source of HONO during the day. Based on the above analysis, we evaluated the contribution of the photo-enhanced heterogeneous pathways.

The coefficients widely adopted in previous studies generally range from 10^{-6} to 10^{-4} (Chen et al., 2023; Liu et al., 2019c; Song et al., 2022; Wong et al., 2013). Here, we used 1 × 10^{-5} as the photo-enhanced uptake coefficients (γ_{a+hv} and γ_{g+hv}) to calculate the $P_{\mathrm{aerosol}+hv}$ and $P_{\mathrm{ground}+hv}$ (Qin et al., 2023; Xue et al., 2020). As shown in Fig. 8, the average $P_{\mathrm{aerosol}+hv}$ and $P_{\mathrm{ground}+hv}$ were 0.02 ± 0.009 ppbv h^{-1} and 0.53 ± 0.50 ppbv h^{-1} during the day, respectively, accounting for 1.4 % and 40.2 % of P_{unknown}, and $P_{\text{aerosol}+h\nu}$ was a negligible source of daytime HONO formation. The photo-enhanced NO_2 heterogeneous reaction on the surfaces matched the calculated P_{unknown} and well-explained the HONO budget in the morning. Furthermore, the higher photo-enhanced uptake coefficient of 3.5×10^{-5} was adopted as the upper limit for calculating the production of photosensitive conversion of NO_2 (Chen et al., 2023). The calculation results demonstrated that the daytime P_{unknown} could be explained when the upper limit of photo-enhanced uptake coefficient was used (Fig. S8).

However, there could be other light-driven reaction pathways to produce HONO in the afternoon, as indicated by the diurnal variation of P_{unknown}. Previous studies have demonstrated that the photolysis of pNO_3/HNO_3 can contribute to HONO production (Chen et al., 2023; Laufs et al., 2017). Recently, Chen et al. (2023) found that the photolysis of HNO_3 at the surface interface could well explain the observed P_{unknown} in the afternoon. However, the lack of information about HNO_3 concentration does not allow us to directly estimate the contribution of HNO_3 photolysis in the present study. Future studies should supplement measurements of pNO_3/HNO_3 to better characterize the contribution of this potentially important HONO formation pathway.

Based on the measured fluxes, we also estimated the HONO emission rate from soil (P_{soil}). The nighttime HONO fluxes ranged from 0.15 nmol m^{-2} s^{-1} to 0.43 nmol m^{-2} s^{-1}, with corresponding HONO flux rates of 0.32 ppbv h^{-1} to 0.79 ppbv h^{-1}, which were fully capable to explaining P_{unknown} (ranging from 0.012 to 0.90 ppbv h^{-1}). Therefore, the light-induced HONO sources (photosensitive conversion of NO_2 and photolysis of pNO_3/HNO_3) and soil emissions could serve together as significant HONO sources in agricultural fields, thereby influencing the overall atmospheric HONO budget.

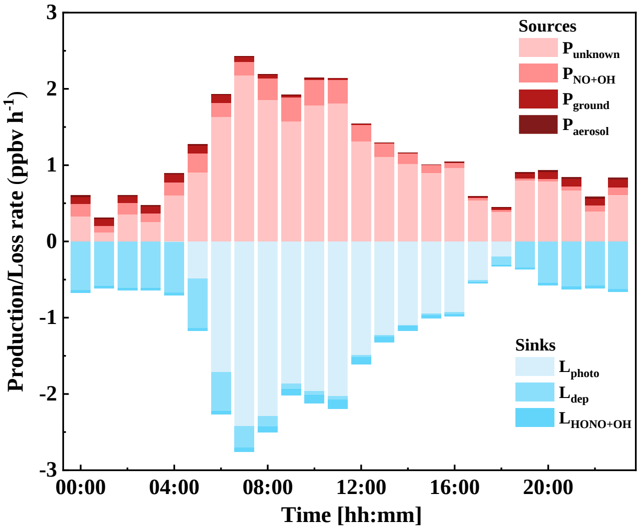

Figure 7. Diurnal variation of HONO budget during rotary tillage.

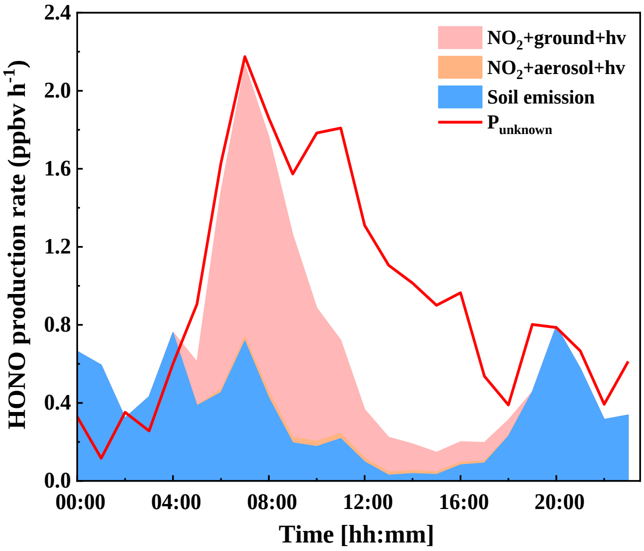

Figure 8. Diurnal variation of light-induced conversion of NO_2 and HONO flux rate derived from soil emission.

3.5 Implication on the atmospheric oxidizing capacity

The significant increase in atmospheric HONO from agricultural fields can enhance the formation of OH radicals via its photolysis (see the detailed OH production rate calculation in Text S4). Figure 9a exhibited the OH production rates from the photolysis of HONO ($P(\mathrm{OH})_{\mathrm{HONO}}$) and O_3 ($P(\mathrm{OH})_{\mathrm{O_3}}$). The $P(\mathrm{OH})_{\mathrm{HONO}}$ and $P(\mathrm{OH})_{\mathrm{O_3}}$ were found to be 0.82 ppbv h^{-1} and 1.49 ppbv h^{-1}, respectively, which were significantly higher than the corresponding winter levels at the same site (Fig. S9). The higher O_3 concentration in summer plays a primary role in the generation of OH radicals by daytime O_3 photolysis, accounting for 70 % of the total OH production rate. However, the contribution of $P(\mathrm{OH})_{\mathrm{HONO}}$, approximately 30 %, is still significant and cannot be ignored.

During the rotary tillage period, continuous peaks in HONO concentration and flux were observed, with maximum values of 3.06 ppbv and 1.86 nmol m^{-2} s^{-1}, respectively. $P(\mathrm{OH})_{\mathrm{HONO}}$ and $P(\mathrm{OH})_{\mathrm{O_3}}$ were calculated to be 1.42 ppbv h^{-1} and 1.35 ppbv h^{-1}, respectively, accounting for 51 % and 49 % of the total OH production rate (Fig. 9b). $P(\mathrm{OH})_{\mathrm{HONO}}$ dominated in the early morning with a value of 2.48 ppbv h^{-1}, while $P(\mathrm{OH})_{\mathrm{O_3}}$ became the main source at midday with a value of 2.74 ppbv h^{-1}. The comparable peak magnitude of $P(\mathrm{OH})_{\mathrm{HONO}}$ and $P(\mathrm{OH})_{\mathrm{O_3}}$ indicates that HONO photolysis is an important source of daytime OH radicals. Furthermore, the peaks of both $P(\mathrm{OH})_{\mathrm{HONO}}$ and HONO flux co-occur in the early morning, revealing the significant contribution of agricultural HONO emissions to the regional atmospheric oxidation capacity in the Huaihe River Basin.

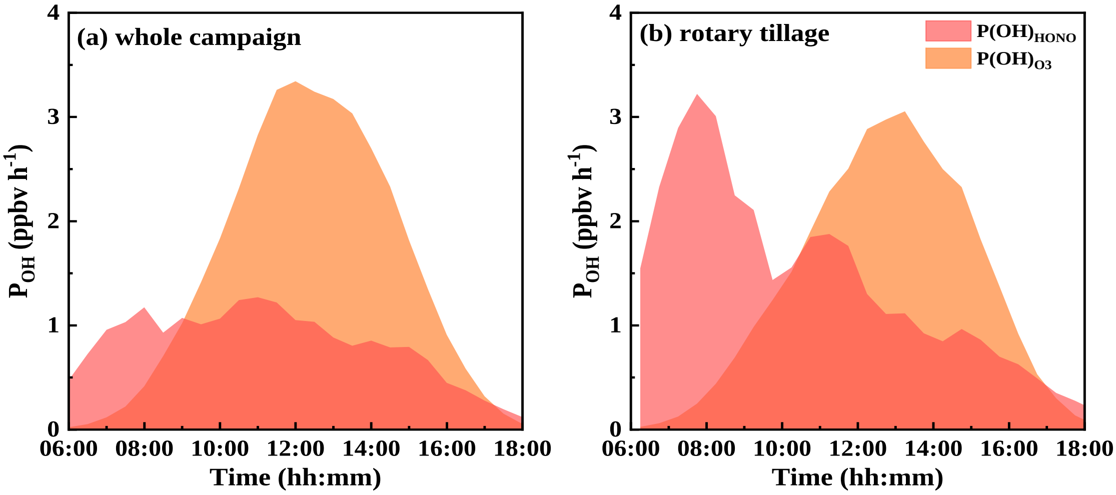

Figure 9. Diurnal variation of net OH production rate of the photolysis of HONO ($P(\mathrm{OH})_{\mathrm{HONO}}$) and O_3 ($P(\mathrm{OH})_{O_3}$) during (a) the whole campaign and (b) the rotary tillage.

4. Conclusion

The extensive agricultural fields and increased agricultural activities have contributed to certain areas in China becoming hotspots for atmospheric nitrogen oxides, underscoring the increasing importance of regional and global nitrogen budgets. However, the available HONO emission fluxes from agricultural soils are relatively limited. In this study, we utilized the AG method to measure the HONO and NO_x fluxes from agricultural fields in the Huaihe River Basin. For HONO and NO, upward fluxes of 0.07 ± 0.22 and 0.19 ± 0.53 nmol m^{-2} s^{-1} were observed, respectively, while NO_2 exhibited a deposition flux to the ground of -0.42 ± 0.44 nmol m^{-2} s^{-1}. The successive peaks in HONO flux and NO flux were measured during rotary tillage, suggesting a potentially enhanced release of HONO and NO due to soil tillage activities. However, the higher WFPS inhibited the microbial nitrification processes after irrigation, leading to a significant decrease in HONO and NO fluxes. Under this inhibitory effect, no significant peaks in HONO flux were observed after fertilization compared with that during the rotary tillage. Considering limited field observation of HONO flux under high soil water content, future studies should pay more attention to paddy fields to validate the mechanisms observed in the laboratory.

Significant fluxes were observed during rotary tillage, prompting the investigation into the HONO sources and budget during this period. Biological processes and light-driven NO_2 reactions on the ground surface may both be sources of HONO and influence the local HONO budget. Higher levels of $P(\mathrm{OH})_{\mathrm{HONO}}$ were observed in the early morning, consistent with the peak emission flux of soil HONO. This reveals the significant contribution of agricultural HONO emissions to the regional atmospheric oxidation capacity in the Huaihe River Basin. Overall, this study provides valuable insights into the dynamics of soil HONO emissions in agricultural fields, elucidating their environmental implications and the role of agricultural activities in the atmospheric chemistry of HONO.

Data availability. The data described in this manuscript are available at https://doi.org/10.5281/zenodo.12738765 (Meng et al., 2024) or upon request from the corresponding author (mqin@aiofm.ac.cn).

Supplement. The supplement related to this article is available online at:

Author contributions. MQ and PX designed the experiments. FM, KT, DS, ZL and JD performed the measurements. FM and BH analyzed the data and wrote the manuscript. MQ revised and commented on the paper. YF, YH and TN provided the ancillary data and experimental sites.

Competing interests. The authors declare that they have no conflict of interest.

Acknowledgements. This work was supported by the National Key Research and Development Program of China (2022YFC3701103), the National Natural Science Foundation of China (U21A2028, 41875154), the Plan for Anhui Major Provincial Science & Technology Project (202203a07020003).

References

Agehara, S. and Warncke, D. D.: Soil Moisture and Temperature Effects on Nitrogen Release from Organic Nitrogen Sources, Soil Sci. Soc. Am. J., 69, 1844-1855, https://doi.org/10.2136/sssaj2004.0361, 2005.

Bargsten, A., Falge, E., Pritsch, K., Huwe, B., and Meixner, F. X.: Laboratory measurements of nitric oxide release from forest soil with a thick organic layer under different understory types, Biogeosciences 7, 1425-1441, https://doi.org/10.5194/bg-7-1425-2010, 2010.

Bejan, I., Abd El Aal, Y., Barnes, I., Benter, T., Bohn, B., Wiesen, P., and Kleffmann, J.: The photolysis of ortho-nitrophenols: a new gas phase source of HONO, Phys. Chem. Chem. Phys., 8, 2028-2035, https://doi.org/10.1039/b516590c, 2006.

Bhattarai, H. R., Wanek, W., Siljanen, H. M. P., Ronkainen, J. G., Liimatainen, M., Hu, Y., Nykänen, H., Biasi, C., and Maljanen, M.: Denitrification is the major nitrous acid production pathway in boreal agricultural soils, Commun. Earth Environ., 2, 54, https://doi.org/10.1038/s43247-021-00125-7, 2021.

Cao, Q., Hao, Z., Yuan, F., Berndtsson, R., Xu, S., Gao, H., and Hao, J.: On the Predictability of Daily Rainfall during Rainy Season over the Huaihe River Basin, Water, 11, 916, https://doi.org/10.3390/w11050916, 2019.

Chatskikh, D. and Olesen, J. E.: Soil tillage enhanced CO_2 and N_2O emissions from loamy sand soil under spring barley, Soil Till. Res., 97, 5-18, https://doi.org/10.1016/j.still.2007.08.004, 2007.

Chen, D., Zhou, L., Liu, S., Lian, C., Wang, W., Liu, H., Li, C., Liu, Y., Luo, L., Xiao, K., Chen, Y., Qiu, Y., Tan, Q., Ge, M., and Yang, F.: Primary sources of HONO vary during the daytime: Insights based on a field campaign, Sci. Total Environ., 903, 166605, https://doi.org/10.1016/j.scitotenv.2023.166605, 2023.

Cheng, P.: Measurement of the atmospheric nitrous acid (HONO) and the study of its soil emissions, Ph.D. Thesis, Peking University, China, 125 pp., 2013.

Duan, J., Qin, M., Ouyang, B., Fang, W., Li, X., Lu, K., Tang, K., Liang, S., Meng, F., Hu, Z., Xie, P., Liu, W., and Häsler, R.: Development of an incoherent broadband cavity-enhanced absorption spectrometer for in situ measurements of HONO and NO_2, Atmos. Meas. Tech., 11, 4531-4543, https://doi.org/10.5194/amt-11-4531-2018, 2018.

Elshorbany, Y. F., Kleffmann, J., Kurtenbach, R., Rubio, M., Lissi, E., Villena, G., Gramsch, E., Rickard, A. R., Pilling, M. J., and Wiesen, P.: Summertime photochemical ozone formation in Santiago, Chile, Atmos. Environ., 43, 6398-6407, https://doi.org/10.1016/j.atmosenv.2009.08.047, 2009.

Ermel, M., Behrendt, T., Oswald, R., Derstroff, B., Wu, D., Hohlmann, S., Stönner, C., Pommerening-Röser, A., Könneke, M., Williams, J., Meixner, F. X., Andreae, M. O., Trebs, I., and Sörgel, M.: Hydroxylamine released by nitrifying microorganisms is a precursor for HONO emission from drying soils, Sci. Rep., 8, 1877, https://doi.org/10.1038/s41598-018-20170-1, 2018.

Fang, S. and Yujing, M.: NO_x fluxes from several typical agricultural fields during summer-autumn in the Yangtze Delta, China, Atmos. Environ., 43, 2665-2671, https://doi.org/10.1016/j.atmosenv.2009.02.027, 2009.

Fang, S., Zhang, Y., and Mu, Y.: Surface-exchange of NO_x and NH_3 above a winter wheat field in the Yangtze Delta, China, J. Environ. Sci., 18, 689-700, 2006.

FAO: World Food and Agriculture – Statistical Yearbook 2022, Rome, https://doi.org/10.4060/cc2211en, 2022.

Feig, G. T., Mamtimin, B., and Meixner, F. X.: Soil biogenic emissions of nitric oxide from a semi-arid savanna in South Africa, Biogeosciences, 5, 1723-1738, https://doi.org/10.5194/bg-5-1723-2008, 2008.

Gan, C., Li, B., Dong, J., Li, Y., Zhao, Y., Wang, T., Yang, Y., and Liao, H.: Atmospheric HONO emissions in China: Unraveling the spatiotemporal patterns and their key influencing factors, Environ. Pollut., 343, 123228, https://doi.org/10.1016/j.envpol.2023.123228, 2024.

Ge, S., Wang, G., Zhang, S., Li, D., Xie, Y., Wu, C., Yuan, Q., Chen, J., and Zhang, H.: Abundant NH$_3$ in China Enhances Atmospheric HONO Production by Promoting the Heterogeneous Reaction of SO$_2$ with NO$_2$, Environ. Sci. Technol., 53, 14339-14347, https://doi.org/10.1021/acs.est.9b04196, 2019.

George, C., Strekowski, R. S., Kleffmann, J., Stemmler, K., and Ammann, M.: Photoenhanced uptake of gaseous NO$_2$ on solid organic compounds: A photochemical source of HONO?, Faraday Discuss., 130, 195-210, https://doi.org/10.1039/b417888m, 2005.

Guo, S. and Li, H.: Photolysis of nitrophenols in gas phase and aqueous environment: a potential daytime source for atmospheric nitrous acid (HONO), Environ. Sci.-Atmos., 3, 143-155, https://doi.org/10.1039/d2ea00053a, 2022.

Han, C., Yang, W., Wu, Q., Yang, H., and Xue, X.: Heterogeneous Photochemical Conversion of NO$_2$ to HONO on the Humic Acid Surface under Simulated Sunlight, Environ. Sci. Technol., 50, 5017-5023, https://doi.org/10.1021/acs.est.5b05101, 2016.

Harrison, R. M. and Kitto, A. M. N.: Evidence for a surface source of atmospheric nitrous acid, Atmos. Environ., 28, 1089-1094, https://doi.org/10.1016/1352-2310(94)90286-0, 1994.

Hu, H. W., Macdonald, C. A., Trivedi, P., Holmes, B., Bodrossy, L., He, J. Z., and Singh, B. K.: Water addition regulates the metabolic activity of ammonia oxidizers responding to environmental perturbations in dry subhumid ecosystems, Environ. Microbiol., 17, 444-461, https://doi.org/10.1111/1462-2920.12481, 2015.

Kim, S., Vandenboer, T. C., Young, C. J., Riedel, T. P., Thornton, J. A., Swarthout, B., Sive, B., Lerner, B., Gilman, J., Warneke, C., Roberts, J. M., Guenther, A., Wagner, N. L., Dubé, W. P., Williams, E., and Brown, S. S.: The primary and recycling sources of OH during the NACHTT-2011 campaign: HONO as an important OH primary source in the wintertime, J. Geophys. Res., 119, 6886-6896, https://doi.org/10.1002/2013JD019784, 2014.

Kirchstetter, T. W., Harley, R. A., and Littlejohn, D.: Measurement of nitrous acid in motor vehicle exhaust, Environ. Sci. Technol., 30, 2843-2849, https://doi.org/10.1021/es960135y, 1996.

Kleffmann, J., Gavriloaiei, T., Hofzumahaus, A., Holland, F., Koppmann, R., Rupp, L., Schlosser, E., Siese, M., and Wahner, A.: Daytime formation of nitrous acid: A major source of OH radicals in a forest, Geophys. Res. Lett., 32, 1-4, https://doi.org/10.1029/2005GL022524, 2005.

Kratz, A. M., Maier, S., Weber, J., Kim, M., Mele, G., Gargiulo, L., Leifke, A. L., Prass, M., Abed, R. M. M., Cheng, Y., Su, H., Pöschl, U., and Weber, B.: Reactive Nitrogen Hotspots Related to Microscale Heterogeneity in Biological Soil Crusts, Environ. Sci. Technol., 56, 11865-11877, https://doi.org/10.1021/acs.est.2c02207, 2022.

Kurtenbach, R., Becker, K. H., Gomes, J. A. G., Kleffmann, J., Lörzer, J. C., Spittler, M., Wiesen, P., Ackermann, R., Geyer, A., and Platt, U.: Investigations of emissions and heterogeneous formation of HONO in a road traffic tunnel, Atmos. Environ., 35, 3385-3394, https://doi.org/10.1016/S1352-2310(01)00138-8, 2001.

Laufs, S., Cazaunau, M., Stella, P., Kurtenbach, R., Cellier, P., Mellouki, A., Loubet, B., and Kleffmann, J.: Diurnal fluxes of HONO above a crop rotation, Atmos. Chem. Phys., 17, 6907-6923, https://doi.org/10.5194/acp-17-6907-2017, 2017.

Lee, J. D., Whalley, L. K., Heard, D. E., Stone, D., Dunmore, R. E., Hamilton, J. F., Young, D. E., Allan, J. D., Laufs, S., and Kleffmann, J.: Detailed budget analysis of HONO in central London reveals a missing daytime source, Atmos. Chem. Phys., 16, 2747-2764, https://doi.org/10.5194/acp-16-2747-2016, 2016.

Li, L., Duan, Z., Li, H., Zhu, C., Henkelman, G., Francisco, J. S., and Zeng, X. C.: Formation of HONO from the NH_3-promoted hydrolysis of NO_2 dimers in the atmosphere, P. Natl. Acad. Sci. USA, 115, 7236-7241, https://doi.org/10.1073/pnas.1807719115, 2018.

Li, X., Brauers, T., Häseler, R., Bohn, B., Fuchs, H., Hofzumahaus, A., Holland, F., Lou, S., Lu, K. D., Rohrer, F., Hu, M., Zeng, L. M., Zhang, Y. H., Garland, R. M., Su, H., Nowak, A., Wiedensohler, A., Takegawa, N., Shao, M., and Wahner, A.: Exploring the atmospheric chemistry of nitrous acid (HONO) at a rural site in Southern China, Atmos. Chem. Phys., 12, 1497-1513, https://doi.org/10.5194/acp-12-1497-2012, 2012.

Liang, Y., Zha, Q., Wang, W., Cui, L., Lui, K. H., Ho, K. F., Wang, Z., Lee, S. C., and Wang, T.: Revisiting nitrous acid (HONO) emission from on-road vehicles: A tunnel study with a mixed fleet, J. Air Waste Manage., 67, 797-805, https://doi.org/10.1080/10962247.2017.1293573, 2017.

Linn, D. M. and Doran, J. W.: Effect of Water-Filled Pore Space on Carbon Dioxide and Nitrous Oxide Production in Tilled and Nontilled Soils, Soil Sci. Soc. Am. J., 48, 1267-1272, https://doi.org/10.2136/sssaj1984.03615995004800060013x, 1984.

Liu, J., Li, S., Mekic, M., Jiang, H., Zhou, W., Loisel, G., Song, W., Wang, X., and Gligorovski, S.: Photoenhanced Uptake of NO_2 and HONO Formation on Real Urban Grime, Environ. Sci. Tech. Let., 6, 413-417, https://doi.org/10.1021/acs.estlett.9b00308, 2019a.

Liu, X. J., Mosier, A. R., Halvorson, A. D., and Zhang, F. S.: Tillage and nitrogen application effects on nitrous and nitric oxide emissions from irrigated corn fields, Plant Soil, 276, 235-249, https://doi.org/10.1007/s11104-005-4894-4, 2005.

Liu, Y., Nie, W., Xu, Z., Wang, T., Wang, R., Li, Y., Wang, L., Chi, X., and Ding, A.: Semi-quantitative understanding of source contribution to nitrous acid (HONO) based on 1 year of continuous observation at the SORPES station in eastern China, Atmos. Chem. Phys., 19, 13289-13308, https://doi.org/10.5194/acp-19-13289-2019, 2019b.

Liu, Y., Lu, K., Ma, Y., Yang, X., Zhang, W., Wu, Y., Peng, J., Shuai, S., Hu, M., and Zhang, Y.: Direct emission of nitrous acid (HONO) from gasoline cars in China determined by vehicle chassis dynamometer experiments, Atmos. Environ., 169, 89-96, https://doi.org/10.1016/j.atmosenv.2017.07.019, 2017.

Liu, Y., Lu, K., Li, X., Dong, H., Tan, Z., Wang, H., Zou, Q., Wu, Y., Zeng, L., Hu, M., Min, K. E., Kecorius, S., Wiedensohler, A., and Zhang, Y.: A Comprehensive Model Test of the HONO Sources Constrained to Field Measurements at Rural North China Plain, Environ. Sci. Technol., 53, 3517-3525, https://doi.org/10.1021/acs.est.8b06367, 2019c.

Ludwig, J., Meixner, F. X., Vogel, B., and Förstner, J.: Soil-air exchange of nitric oxide: An overview of processes, environmental factors, and modeling studies, Biogeochemistry, 52, 225-257, https://doi.org/10.1023/A:1006424330555, 2001.

Mamtimin, B., Meixner, F. X., Behrendt, T., Badawy, M., and Wagner, T.: The contribution of soil biogenic NO and HONO emissions from a managed hyperarid ecosystem to the regional NO_x emissions during growing season, Atmos. Chem. Phys., 16, 10175-10194, https://doi.org/10.5194/acp-16-10175-2016, 2016.

Marion, A., Morin, J., Gandolfo, A., Ormeño, E., D'Anna, B., and Wortham, H.: Nitrous acid formation on Zea mays leaves by heterogeneous reaction of nitrogen dioxide in the laboratory, Environ. Res., 193, https://doi.org/10.1016/j.envres.2020.110543, 2021.

Meng, F., Qin, M., Fang, W., Duan, J., Tang, K., Zhang, H., Shao, D., Liao, Z., Feng, Y., Huang, Y., Ni, T., Xie, P., Liu, J., and Liu, W.: Measurement of HONO flux using the aerodynamic gradient method over an agricultural field in the Huaihe River Basin, China, J. Environ. Sci., 114, 297-307, https://doi.org/10.1016/j.jes.2021.09.005, 2022.

Meng, F., Han, B., Qin, M., Fang, W., Tang, K., Shao, D., Liao, Z., Duan, J., Feng, Y., Huang, Y., Ni, T., Xie, P.: Measurement report: Surface exchange fluxes of HONO during the growth process of paddy fields in the Huaihe River Basin, China, Zenodo [Data set], https://doi.org/10.5281/zenodo.12738765, 2024.

Meusel, H., Tamm, A., Kuhn, U., Wu, D., Lena Leifke, A., Fiedler, S., Ruckteschler, N., Yordanova, P., Lang-Yona, N., Pöhlker, M., Lelieveld, J., Hoffmann, T., Pöschl, U., Su, H., Weber, B., and Cheng, Y.: Emission of nitrous acid from soil and biological soil crusts represents an important source of HONO in the remote atmosphere in Cyprus, Atmos. Chem. Phys., 18, 799-813, https://doi.org/10.5194/acp-18-799-2018, 2018.

Monge, M. E., D'Anna, B., Mazri, L., Giroir-Fendler, A., Ammann, M., Donaldson, D. J., and George, C.: Light changes the atmospheric reactivity of soot, P. Natl. Acad. Sci. USA, 107, 6605-6609, https://doi.org/10.1073/pnas.0908341107, 2010.

Monks, P. S., Granier, C., Fuzzi, S., Stohl, A., Williams, M. L., Akimoto, H., Amann, M., Baklanov, A., Baltensperger, U., Bey, I., Blake, N., Blake, R. S., Carslaw, K., Cooper, O. R., Dentener, F., Fowler, D., Fragkou, E., Frost, G. J., Generoso, S., Ginoux, P., Grewe, V., Guenther, A., Hansson, H. C., Henne, S., Hjorth, J., Hofzumahaus, A., Huntrieser, H., Isaksen, I. S. A., Jenkin, M. E., Kaiser, J., Kanakidou, M., Klimont, Z., Kulmala, M., Laj, P., Lawrence, M. G., Lee, J. D., Liousse, C., Maione, M., McFiggans, G., Metzger, A., Mieville, A., Moussiopoulos, N., Orlando, J. J., O'Dowd, C. D., Palmer, P. I., Parrish, D. D., Petzold, A., Platt, U., Pöschl, U., Prévôt, A. S. H., Reeves, C. E., Reimann, S., Rudich, Y., Sellegri, K., Steinbrecher, R., Simpson, D., ten Brink, H., Theloke, J., van der Werf, G. R., Vautard, R., Vestreng, V., Vlachokostas, C., and von Glasow, R.: Atmospheric composition change - global and regional air quality, Atmos. Environ., 43, 5268-5350, https://doi.org/10.1016/j.atmosenv.2009.08.021, 2009.

Mueller, N. D., Lassaletta, L., Runck, B. C., Billen, G., Garnier, J., and Gerber, J. S.: Declining spatial efficiency of global cropland nitrogen allocation, Global Biogeochem. Cy., 31, 245-257, https://doi.org/10.1002/2016gb005515, 2017.

Nakashima, Y. and Kajii, Y.: Determination of nitrous acid emission factors from a gasoline vehicle using a chassis dynamometer combined with incoherent broadband cavity-enhanced absorption spectroscopy, Sci. Total Environ., 575, 287-293, https://doi.org/10.1016/j.scitotenv.2016.10.050, 2017.

Nakashima, Y. and Kondo, Y.: Nitrous acid (HONO) emission factors for diesel vehicles determined using a chassis dynamometer, Sci. Total Environ., 806, 150927, https://doi.org/10.1016/j.scitotenv.2021.150927, 2022.

Nan, J., Wang, S., Guo, Y., Xiang, Y., and Zhou, B.: Study on the daytime OH radical and implication for its relationship with fine particles over megacity of Shanghai, China, Atmos. Environ., 154, 167-178, https://doi.org/10.1016/j.atmosenv.2017.01.046, 2017.

Ndour, M., D'Anna, B., George, C., Ka, O., Balkanski, Y., Kleffmann, J., Stemmler, K., and Ammann, M.: Photoenhanced uptake of NO_2 on mineral dust: Laboratory experiments and model simulations, Geophys. Res. Lett., 35, L05812, https://doi.org/10.1029/2007gl032006, 2008.

Nie, W., Ding, A. J., Xie, Y. N., Xu, Z., Mao, H., Kerminen, V. M., Zheng, L. F., Qi, X. M., Huang, X., Yang, X. Q., Sun, J. N., Herrmann, E., Petäjä, T., Kulmala, M., and Fu, C. B.: Influence of biomass burning plumes on HONO chemistry in eastern China, Atmos. Chem. Phys., 15, 1147-1159, https://doi.org/10.5194/acp-15-1147-2015, 2015.

Oswald, R., Behrendt, T., Ermel, M., Wu, D., Su, H., Cheng, Y., Breuninger, C., Moravek, A., Mougin, E., Delon, C., Loubet, B., Pommerening-Roser, A., Sorgel, M., Poschl, U., Hoffmann, T., Andreae, M. O., Meixner, F. X., and Trebs, I.: HONO emissions from soil bacteria as a major source of atmospheric reactive nitrogen, Science, 341, 1233-1235, https://doi.org/10.1126/science.1242266, 2013.

Pilegaard, K.: Processes regulating nitric oxide emissions from soils, Philos. T. Roy. Soc. B, 368, https://doi.org/10.1098/rstb.2013.0126, 2013.

Pinto, M., Merino, P., del Prado, A., Estavillo, J. M., Yamulki, S., Gebauer, G., Piertzak, S., Lauf, J., and Oenema, O.: Increased emissions of nitric oxide and nitrous oxide following tillage of a perennial pasture, Nutr. Cycl. Agroecosys., 70, 13-22, https://doi.org/10.1023/B:FRES.0000049357.79307.23, 2004.

Qin, Z., Geng, C., Xu, B., Liu, Y., Zhang, N., Zheng, Z., Wang, X., and Yang, W.: Springtime HONO budget and its impact on the O_3 production in Zibo, Shandong, China, Atmos. Pollut. Res., 15, 101935, https://doi.org/10.1016/j.apr.2023.101935, 2023.

Ren, X., Sanders, J. E., Rajendran, A., Weber, R. J., Goldstein, A. H., Pusede, S. E., Browne, E. C., Min, K. E., and Cohen, R. C.: A relaxed eddy accumulation system for measuring vertical fluxes of nitrous acid, Atmos. Meas. Tech., 4, 2093-2103, https://doi.org/10.5194/amt-4-2093-2011, 2011.

Rende, A., Slemr, F., and Conrad, R.: Microbial production and uptake of nitric oxide in soil, FEMS Microbiol. Ecol., 62, 221-230, https://doi.org/10.1111/j.1574-6968.1989.tb03696.x, 1989.

Scharko, N. K., Schütte, U. M. E., Berke, A. E., Banina, L., Peel, H. R., Donaldson, M. A., Hemmerich, C., White, J. R., and Raff, J. D.: Combined Flux Chamber and Genomics Approach Links Nitrous Acid Emissions to Ammonia Oxidizing Bacteria and Archaea in Urban and Agricultural Soil, Environ. Sci. Technol., 49, 13825-13834, https://doi.org/10.1021/acs.est.5b00838, 2015.

Sehy, U., Ruser, R., and Munch, J. C.: Nitrous oxide fluxes from maize fields: relationship to yield, site-specific fertilization, and soil conditions, Agr. Ecosyst. Environ., 99, 97-111, https://doi.org/10.1016/s0167-8809(03)00139-7, 2003.

Skiba, U., Smith, K. A., and Fowler, D.: Nitrification and denitrification as sources of nitric oxide and nitrous oxide in a sandy loam soil, Soil Biol. Biochem., 25, 1527-1536, https://doi.org/10.1016/0038-0717(93)90007-X, 1993.

Song, Y., Xue, C., Zhang, Y., Liu, P., Bao, F., Li, X., and Mu, Y.: Measurement report: Exchange fluxes of HONO over agricultural fields in the North China Plain, Atmos. Chem. Phys., 23, 15733-15747, https://doi.org/10.5194/acp-23-15733-2023, 2023.

Song, Y., Zhang, Y., Xue, C., Liu, P., He, X., Li, X., and Mu, Y.: The seasonal variations and potential sources of nitrous acid (HONO) in the rural North China Plain, Environ. Pollut., 311, 119967, https://doi.org/10.1016/j.envpol.2022.119967, 2022.

Sörgel, M., Trebs, I., Wu, D., and Held, A.: A comparison of measured HONO uptake and release with calculated source strengths in a heterogeneous forest environment, Atmos. Chem. Phys., 15, 9237-9251, https://doi.org/10.5194/acp-15-9237-2015, 2015.

Sörgel, M., Regelin, E., Bozem, H., Diesch, J. M., Drewnick, F., Fischer, H., Harder, H., Held, A., Hosaynali-Beygi, Z., Martinez, M., and Zetzsch, C.: Quantification of the unknown HONO daytime source and its relation to NO_2, Atmos. Chem. Phys., 11, 10433-10447, https://doi.org/10.5194/acp-11-10433-2011, 2011.

Stella, P., Loubet, B., Laville, P., Lamaud, E., Cazaunau, M., Laufs, S., Bernard, F., Grosselin, B., Mascher, N., Kurtenbach, R., Mellouki, A., Kleffmann, J., and Cellier, P.: Comparison of methods for the determination of NO-O_3-NO_2 fluxes and chemical interactions over a bare soil, Atmos. Meas. Tech., 5, 1241-1257, https://doi.org/10.5194/amt-5-1241-2012, 2012.

Stemmler, K., Ammann, M., Donders, C., Kleffmann, J., and George, C.: Photosensitized reduction of nitrogen dioxide on humic acid as a source of nitrous acid, Nature, 440, 195-198, https://doi.org/10.1038/nature04603, 2006.

Su, H., Cheng, Y., Oswald, R., Behrendt, T., Trebs, I., Meixner, F. X., Andreae, M. O., Cheng, P., Zhang, Y., and Pöschl, U.: Soil nitrite as a source of atmospheric HONO and OH radicals, Science, 333, 1616-1618, https://doi.org/10.1126/science.1207687, 2011.

Su, H., Cheng, Y. F., Cheng, P., Zhang, Y. H., Dong, S., Zeng, L. M., Wang, X., Slanina, J., Shao, M., and Wiedensohler, A.: Observation of nighttime nitrous acid (HONO) formation at a non-urban site during PRIDE-PRD2004 in China, Atmos. Environ., 42, 6219-6232, https://doi.org/10.1016/j.atmosenv.2008.04.006, 2008.

Sutton, M. A., Fowler, D., and Moncrieff, J. B.: The exchange of atmospheric ammonia with vegetated surfaces. I: Unfertilized vegetation, Q. J. Roy. Meteor. Soc., 119, 1023-1045, https://doi.org/10.1016/S1352-2310(97)00164-7, 1993.

Tang, K., Qin, M., Duan, J., Fang, W., Meng, F., Liang, S., Xie, P., Liu, J., Liu, W., Xue, C., and Mu, Y.: A dual dynamic chamber system based on IBBCEAS for measuring fluxes of nitrous acid in agricultural fields in the North China Plain, Atmos. Environ., 196, 10-19, https://doi.org/10.1016/j.atmosenv.2018.09.059, 2019.

Tang, K., Qin, M., Fang, W., Duan, J., Meng, F., Ye, K., Zhang, H., Xie, P., Liu, J., Liu, W., Feng, Y., Huang, Y., and Ni, T.: An automated dynamic chamber system for exchange flux measurement of reactive nitrogen oxides (HONO and NO_x) in farmland ecosystems of the Huaihe River Basin, China, Sci. Total Environ., 745, 140867, https://doi.org/10.1016/j.scitotenv.2020.140867, 2020.

Tang, Y., An, J., Wang, F., Li, Y., Qu, Y., Chen, Y., and Lin, J.: Impacts of an unknown daytime HONO source on the mixing ratio and budget of HONO, and hydroxyl, hydroperoxyl, and organic peroxy radicals, in the coastal regions of China, Atmos. Chem. Phys., 15, 9381-9398, https://doi.org/10.5194/acp-15-9381-2015, 2015.

Vandenboer, T. C., Young, C. J., Talukdar, R. K., Markovic, M. Z., Brown, S. S., Roberts, J. M., and Murphy, J. G.: Nocturnal loss and daytime source of nitrous acid through reactive uptake and displacement, Nat. Geosci., 8, 55-60, https://doi.org/10.1038/ngeo2298, 2015.

VandenBoer, T. C., Markovic, M. Z., Sanders, J. E., Ren, X., Pusede, S. E., Browne, E. C., Cohen, R. C., Zhang, L., Thomas, J., Brune, W. H., and Murphy, J. G.: Evidence for a nitrous acid (HONO) reservoir at the ground surface in Bakersfield, CA, during CalNex 2010, J. Geophy. Res., 119, 9093-9106, https://doi.org/10.1002/2013JD020971, 2014.

Vandenboer, T. C., Brown, S. S., Murphy, J. G., Keene, W. C., Young, C. J., Pszenny, A. A. P., Kim, S., Warneke, C., De Gouw, J. A., Maben, J. R., Wagner, N. L., Riedel, T. P., Thornton, J. A., Wolfe, D. E., Dubé, W. P., Öztürk, F., Brock, C. A., Grossberg, N., Lefer, B., Lerner, B., Middlebrook, A. M., and Roberts, J. M.: Understanding the role of the ground surface in HONO vertical structure: High resolution vertical profiles during NACHTT-11, J. Geophys. Res.-Atmos., 118, 10155-10171, https://doi.org/10.1002/jgrd.50721, 2013.

Von Der Heyden, L., Wißdorf, W., Kurtenbach, R., and Kleffmann, J.: A relaxed eddy accumulation (REA) LOPAP system for flux measurements of nitrous acid (HONO), Atmos. Meas. Tech., 15, 1983-2000, https://doi.org/10.5194/amt-15-1983-2022, 2022.

Wang, Y., Fu, X., Wu, D., Wang, M., Lu, K., Mu, Y., Liu, Z., Zhang, Y., and Wang, T.: Agricultural Fertilization Aggravates Air Pollution by Stimulating Soil Nitrous Acid Emissions at High Soil Moisture, Environ. Sci. Technol., 55, 14556-14566, https://doi.org/10.1021/acs.est.1c04134, 2021.

Weber, B., Wu, D., Tamm, A., Ruckteschler, N., Rodríguez-Caballero, E., Steinkamp, J., Meusel, H., Elbert, W., Behrendt, T., Sörgel, M., Cheng, Y., Crutzen, P. J., Su, H., Pöschl, U., and Wofsy, S. C.: Biological soil crusts accelerate the nitrogen cycle through large NO and HONO emissions in drylands, P. Natl. Acad. Sci. USA, 112, 15384-15389, https://doi.org/10.1073/pnas.1515818112, 2015.

Wong, K. W., Tsai, C., Lefer, B., Grossberg, N., and Stutz, J.: Modeling of daytime HONO vertical gradients during SHARP 2009, Atmos. Chem. Phys., 13, 3587-3601, https://doi.org/10.5194/acp-13-3587-2013, 2013.

Wu, D., Kampf, C. J., Pöschl, U., Oswald, R., Cui, J., Ermel, M., Hu, C., Trebs, I., and Sörgel, M.: Novel tracer method to measure isotopic labeled gas-phase nitrous acid ($HO^{15}NO$) in biogeochemical studies, Environ. Sci. Technol., 48, 8021-8027, https://doi.org/10.1021/es501353x, 2014.

Wu, D., Horn, M. A., Behrendt, T., Müller, S., Li, J., Cole, J. A., Xie, B., Ju, X., Li, G., Ermel, M., Oswald, R., Fröhlich-Nowoisky, J., Hoor, P., Hu, C., Liu, M., Andreae, M. O., Pöschl, U., Cheng, Y., Su, H., Trebs, I., Weber, B., and Sörgel, M.: Soil HONO emissions at high moisture content are driven by microbial nitrate reduction to nitrite: tackling the HONO puzzle, ISME J., 13, 1688-1699, https://doi.org/10.1038/s41396-019-0379-y, 2019.

Wu, D., Zhang, J., Wang, M., An, J., Wang, R., Haider, H., Huang, Y., Zhang, Q., Zhou, F., Tian, H., Zhang, X., Deng, L., Pan, Y., Chen, X., Yu, Y., Hu, C., Wang, R., Song, Y., Gao, Z., Wang, Y., Hou, L., and Liu, M.: Global and Regional Patterns of Soil Nitrous Acid Emissions and Their Acceleration of Rural Photochemical Reactions, J. Geophys. Res.-Atmos., 127, e2021JD036379, https://doi.org/10.1029/2021JD036379, 2022.

Xu, W., Kuang, Y., Zhao, C., Tao, J., Zhao, G., Bian, Y., Yang, W., Yu, Y., Shen, C., Liang, L., Zhang, G., Lin, W., and Xu, X.: NH_3-promoted hydrolysis of NO_2 induces explosive growth in HONO, Atmos. Chem. Phys., 19, 10557-10570, https://doi.org/10.5194/acp-19-10557-2019, 2019.

Xue, C., Ye, C., Zhang, Y., Ma, Z., Liu, P., Zhang, C., Zhao, X., Liu, J., and Mu, Y.: Development and application of a twin open-top chambers method to measure soil HONO emission in the North China Plain, Sci. Total Environ., 659, 621-631, https://doi.org/10.1016/j.scitotenv.2018.12.245, 2019.

Xue, C., Ye, C., Kleffmann, J., Zhang, W., He, X., Liu, P., Zhang, C., Zhao, X., Liu, C., Ma, Z., Liu, J., Wang, J., Lu, K., Catoire, V., Mellouki, A., and Mu, Y.: Atmospheric measurements at Mt. Tai - Part II: HONO budget and radical (RO_x+NO_3) chemistry in the lower boundary layer, Atmos. Chem. Phys., 22, 1035-1057, https://doi.org/10.5194/acp-22-1035-2022, 2022.

Xue, C., Ye, C., Lu, K., Liu, P., Zhang, C., Su, H., Bao, F., Cheng, Y., Wang, W., Liu, Y., Catoire, V., Ma, Z., Zhao, X., Song, Y., Ma, X., McGillen, M. R., Mellouki, A., Mu, Y., and Zhang, Y.: Reducing Soil-Emitted Nitrous Acid as a Feasible Strategy for Tackling Ozone Pollution, Environ. Sci. Technol., 58, 9227-9235, https://doi.org/10.1021/acs.est.4c01070, 2024.

Xue, C., Zhang, C., Ye, C., Liu, P., Catoire, V., Krysztofiak, G., Chen, H., Ren, Y., Zhao, X., Wang, J., Zhang, F., Zhang, C., Zhang, J., An, J., Wang, T., Chen, J., Kleffmann, J., Mellouki, A., and Mu, Y.: HONO budget and its role in nitrate formation in the rural North China Plain, Environ. Sci. Technol., 54, 11048-11057, https://doi.org/10.1021/acs.est.0c01832, 2020.

Yamulki, S. and Jarvis, S. C.: Short-term effects of tillage and compaction on nitrous oxide, nitric oxide, nitrogen dioxide, methane and carbon dioxide fluxes from grassland, Biol. Fert. Soils, 36, 224-231, https://doi.org/10.1007/s00374-002-0530-0, 2002.

Yao, Z., Zheng, X., Xie, B., Mei, B., Wang, R., Butterbach-Bahl, K., Zhu, J., and Yin, R.: Tillage and crop residue management significantly affects N-trace gas emissions during the non-rice season of a subtropical rice-wheat rotation, Soil Biol. Biochem., 41, 2131-2140, https://doi.org/10.1016/j.soilbio.2009.07.025, 2009.

Ye, C., Zhang, N., Gao, H., and Zhou, X.: Photolysis of Particulate Nitrate as a Source of HONO and NO_x, Environ. Sci. Technol., 51, 6849-6856, https://doi.org/10.1021/acs.est.7b00387, 2017.

Ye, C., Lu, K., Ma, X., Qiu, W., Li, S., Yang, X., Xue, C., Zhai, T., Liu, Y., Li, X., Li, Y., Wang, H., Tan, Z., Chen, X., Dong, H., Zeng, L., Hu, M., and Zhang, Y.: HONO chemistry at a suburban site during the EXPLORE-YRD campaign in 2018: formation mechanisms and impacts on O_3 production, Atmos. Chem. Phys., 23, 15455-15472, https://doi.org/10.5194/acp-23-15455-2023, 2023.

Zhang, N., Zhou, X., Bertman, S., Tang, D., Alaghmand, M., Shepson, P. B., and Carroll, M. A.: Measurements of ambient HONO concentrations and vertical HONO flux above a northern Michigan forest canopy, Atmos. Chem. Phys., 12, 8285-8296, https://doi.org/10.5194/acp-12-8285-2012, 2012.

Zhang, X., Davidson, E. A., Mauzerall, D. L., Searchinger, T. D., Dumas, P., and Shen, Y.: Managing nitrogen for sustainable development, Nature, 528, 51-59, https://doi.org/10.1038/nature15743, 2015.

Zhou, X., Gao, H., He, Y., Huang, G., Bertman, S. B., Civerolo, K., and Schwab, J.: Nitric acid photolysis on surfaces in low-NO_x environments: Significant atmospheric implications, Geophys. Res. Lett., 30, 2217, https://doi.org/10.1029/2003GL018620, 2003.

Zhou, X., Zhang, N., Teravest, M., Tang, D., Hou, J., Bertman, S., Alaghmand, M., Shepson, P. B., Carroll, M. A., Griffith, S., Dusanter, S., and Stevens, P. S.: Nitric acid photolysis on forest canopy surface as a source for tropospheric nitrous acid, Nat. Geosci., 4, 440-443, https://doi.org/10.1038/ngeo1164, 2011.